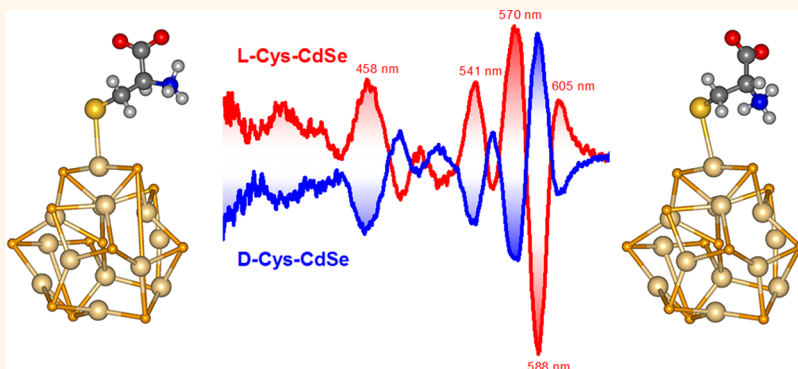


# Ligand Induced Circular Dichroism and Circularly Polarized Luminescence in CdSe Quantum Dots

Urice Tohgha,<sup>†</sup> Kirandeep K. Deol,<sup>‡</sup> Ashlin G. Porter,<sup>†</sup> Samuel G. Bartko,<sup>†</sup> Jung Kyu Choi,<sup>†</sup> Brian M. Leonard,<sup>†</sup> Krisztina Varga,<sup>†</sup> Jan Kubelka,<sup>†</sup> Gilles Muller,<sup>‡,\*</sup> and Milan Balaz<sup>†,\*</sup>

<sup>†</sup>Department of Chemistry, University of Wyoming, 1000 East University Avenue, Laramie, Wyoming 82071, United States, and <sup>‡</sup>Department of Chemistry, San José State University, San José, California 95192-0101, United States

## ABSTRACT



Chiral thiol capping ligands L- and D-cysteines induced modular chiroptical properties in achiral cadmium selenide quantum dots (CdSe QDs). Cys-CdSe prepared from achiral oleic acid capped CdSe by postsynthetic ligand exchange displayed size-dependent electronic circular dichroism (CD) and circularly polarized luminescence (CPL). Opposite CPL signals were measured for the CdSe QDs capped with D- and L-cysteine. The CD profile and CD anisotropy varied with size of CdSe nanocrystals with largest anisotropy observed for CdSe nanoparticles of 4.4 nm. Magic angle spinning solid state NMR (MAS ssNMR) experiments suggested bidentate interaction between cysteine and the surface of CdSe. Time Dependent Density Functional Theory (TDDFT) calculations verified that attachment of L- and D-cysteine to the surface of model (CdSe)<sub>13</sub> nanoclusters induces measurable opposite CD signals for the excitonic band of the nanocluster. The origin of the induced chirality is consistent with the hybridization of highest occupied CdSe molecular orbitals with those of the chiral ligand.

**KEYWORDS:** chiral quantum dots · chiral cadmium selenide · optical activity · induced circular dichroism · circularly polarized luminescence · solid state NMR · TDDFT calculation

**C**hiral optically active semiconductor and metallic nanoparticles possess unique yet modular structural and optical properties not present in bulk materials.<sup>1–5</sup> Nanoparticles are promising candidates for a broad range of applications such as biosensing, labeling, environmental nanoassays and chiral memory as well as attractive building blocks for the bottom-up nanofabrication of chiroptical devices and nanoassemblies.<sup>6–9</sup> Chiroptical activity in semiconductor and metallic nanoparticles can originate from several distinct phenomena that can concurrently affect the resulting chiroptical properties.<sup>1</sup> The nanocrystals can be intrinsically chiral with mirror-image

arrangement of atoms within the crystals.<sup>10–13</sup> Chiroptical activity of nanocrystals can also be induced by a chiral environment *via* binding of chiral organic ligands to the surface<sup>14–19</sup> or *via* an electronic coupling between nanocrystal and chiral ligands in its proximity.<sup>3,13,15,20,21</sup> Coupled with quantum size effect, the postsynthetic ligand exchange introducing a chiral organic shell represents an appealing approach to induce and tune optical and chiroptical characteristics of achiral quantum dots (QDs). Importantly, organic capping ligands can be used to trigger and control interactions and self-assembly of optically active nanoparticles.

Chiral optically active QDs have been traditionally synthesized from their precursors

\*Address correspondence to  
gilles.muller@sjsu.edu,  
mbalaz@uwyo.edu.

Received for review September 16, 2013  
and accepted November 7, 2013.

Published online November 07, 2013  
10.1021/nn404832f

© 2013 American Chemical Society

in the presence of chiral ligands<sup>8,16,22–24</sup> or within a protein cavity.<sup>25</sup> We have recently reported a novel approach for the preparation of optically active QDs: introduction of L- and D-cysteine ligands on the surface of achiral cadmium selenide quantum dots (CdSe QDs) induced mirror-image CD spectra.<sup>17</sup> Herein we report the size and ligand dependent chiroptical and anisotropy properties studied by circular dichroism, fluorescence detected circular dichroism (FDCD), and circularly polarized luminescence. Magic angle spinning solid state NMR (MAS ssNMR) spectroscopy has been utilized to evaluate conformational behavior of the cysteine capping ligand and its interaction with CdSe surface. Time Dependent Density Functional Theory (TDDFT) calculations have been employed to further rationalize the origin of induced chiroptical signal.

## RESULTS AND DISCUSSION

**Synthesis and TEM of Cysteine-CdSe QDs.** Oleic acid capped CdSe QDs (OA-CdSe) and trioctylphosphine-oxide (TOPO)-OA capped CdSe QDs (TOPO/OA-CdSe) have been synthesized by hot injection. Their diameters have been calculated from Peng's equation.<sup>26</sup> The L- and D-cysteine-capped CdSe QDs have been prepared from OA-CdSe and TOPO/OA-CdSe QDs by phase transfer ligand exchange. Experimental details of all synthetic procedures can be found in Supporting Information. The ligand exchange caused a 1–3 nm blue shift of the excitonic band absorption maxima (see Supporting Information, Table S3). High resolution transition electron microscopy (HRTEM) images of OA-CdSe QDs (diameter = 2.9 nm) and corresponding L-cysteine-CdSe QDs have been collected (Figure 1). TEM images of L-Cys-CdSe have revealed formation of closely packed QDs clusters while well separated QD nanoparticles have been observed for OA-CdSe. Long hydrophobic OA chains kept CdSe QDs farther apart than short charged cysteine ligands. Similar behavior may exist in solution.

**Electronic Circular Dichroism and Fluorescence Detected Circular Dichroism.** The electronic CD spectra of L-cysteine- and D-cysteine- capped CdSe QDs prepared from OA-CdSe as well as from TOPO/OA-CdSe exhibited mirror-image profiles (Figure 2). However, several differences could be observed. The CD spectrum of L-Cys-CdSe prepared from TOPO/OA-CdSe displayed a strong bisignate CD feature around the band gap absorption region with a negative Cotton effect at 534.8 nm and a positive Cotton effect at 517.2 nm. On the other hand, the CD spectrum of L-Cys-CdSe prepared from OA-CdSe exhibited a strong trisignate CD feature within the band gap region with positive Cotton effects at 553.5 and 518.0 nm and a negative Cotton effect at 535.0 nm. The comparison of the CD spectra clearly showed appearance of a new CD band at longer wavelengths and more intense CD signal at shorter wavelengths (<450 nm) in the CdSe prepared from OA-CdSe.

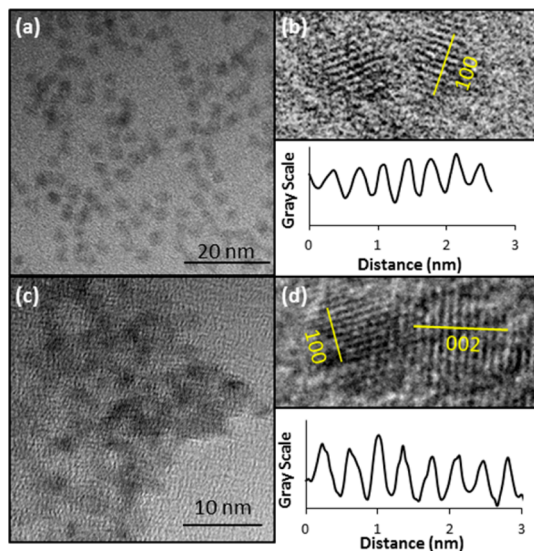


Figure 1. TEM images of (a and b) oleic acid capped CdSe, and (c and d) optically active L-cysteine capped CdSe QDs. Diameter (CdSe) = 2.9 nm. The inset profiles confirm the 100 lattice spacing of 3.7 Å.

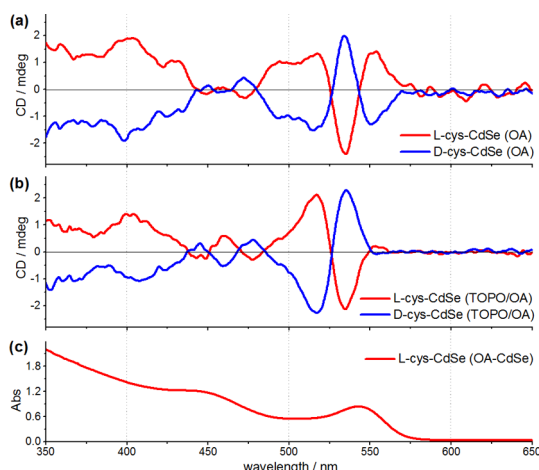
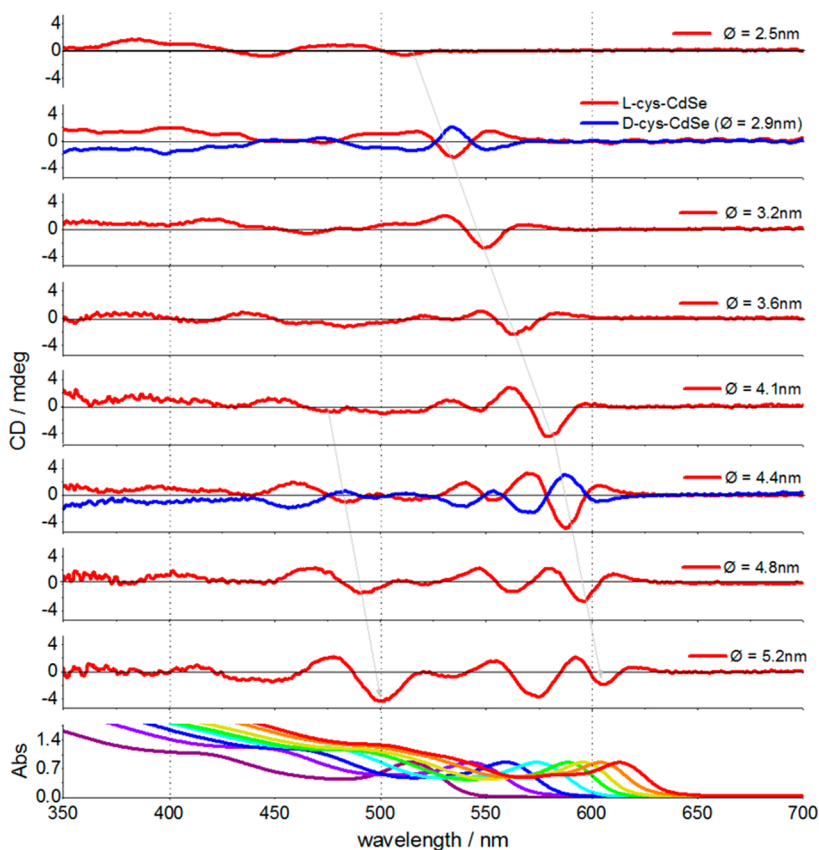


Figure 2. (a and b) CD and (c) UV-vis absorption spectra of L-Cys-CdSe (red curves) and D-Cys-CdSe (blue curves) prepared from OA-CdSe (top spectrum) and from TOPO/OA-CdSe (middle spectrum).  $\phi = 2.9$  nm.  $[Cys-CdSe] = 8.58 \mu M$  ( $A(\lambda_{exc}) = 0.85$ ).

The CD data showed that the synthetic origin of the CdSe QDs (i.e., type of capping ligands) influence the cysteine-induced CD spectra. We postulate that different CD spectra originated as a combination of different ligand coverage and different atomic surface structure in TOPO/OA-CdSe and OA-CdSe QDs. This phenomenon provides the possibility to further modulate the induced chiroptical properties of cysteine-CdSe QDs. FDCD has been previously used to evaluate the structural properties of chiral penicillamine-CdSe QDs prepared by direct aqueous synthesis.<sup>27</sup> The FDCD measurement were performed on Jasco J-815 spectropolarimeter equipped FDCD attachment with ellipsoidal mirror structure that maximally collects light in the FDCD and eliminates



**Figure 3.** (Top) Size-dependent CD spectra of L-Cys-CdSe (red curves) and D-Cys-CdSe (blue curves) prepared from OA-CdSe. (Bottom spectrum) Size dependent UV-vis absorption profiles of different diameters of L-Cys-CdSe QDs. All spectra were measured for solutions of absorbance  $A(\lambda_{\text{exc}}) = 0.85$ . Concentrations of Cys-CdSe can be found in Table S3.

the polarization artifacts.<sup>28</sup> Unfortunately, FDCD spectra of L-Cys- and D-Cys-CdSe QDs ( $\phi = 2.9$  nm) did not show any detectable chiroptical signal (Supporting Information, Figure S11). The lack of the FDCD signal could have been caused by very low fluorescence signal of cysteine-capped CdSe QDs.

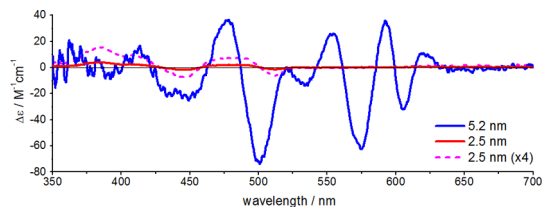
Similarly to absorption and emission spectra (Figures S1–S9), cysteine-capped CdSe also exhibited size dependent CD characteristics. As shown in Figure 3, the increase of diameter caused a bathochromic shift of the Cotton effects. The CD experiments were performed at identical absorbance of the excitonic band ( $A(\lambda_{\text{max}}) = 0.85$ ). With increasing size of L-Cys-CdSe nanoparticles, a progressive spectral change has been observed. New CD bands started to appear at shorter wavelengths at diameter  $\geq 4.1$  nm. The strongest Cotton effect at the band gap wavelengths have been observed for L-Cys-CdSe with 4.4 nm in diameter.

To evaluate the influence of the nanoparticle size on the dissymmetry of the L-cysteine-capped CdSe, we calculated their CD anisotropy factors (also known as Kuhn's dissymmetry ratio,  $g$ ). The CD anisotropy factor is defined as  $g = \Delta\epsilon/\epsilon = (A_L - A_R)/A$  where  $A$  represents the conventional absorbance of nonpolarized light and  $A_L$  and  $A_R$  are the absorptions of left and right circularly

polarized light, respectively. The CD anisotropy factor is independent of the concentration and of the path length if the CD and absorbance spectra are taken on the same sample. CD anisotropy values of L-Cys-CdSe QDs for the two most intense CD bands (one positive and one negative Cotton effect) are summarized in Table 1. Markovich and collaborators have reported a strong dependence of CD anisotropy at the excitonic wavelength on the diameter of penicillamine-CdSe with largest dissymmetry values ( $\approx -8 \times 10^{-4}$ ) as shown for smallest CdSe nanoparticles ( $D = 1.2$  nm). Larger penicillamine-CdSe QDs ( $D = 1.7$  and  $1.9$  nm) exhibited much smaller anisotropy values ( $g_{\text{CD}} < -2 \times 10^{-4}$ ). Larger chiral CdSe prepared by aqueous synthesis have not been studied. In our study, the cysteine capping ligands induced anisotropy in all studied sizes of cysteine-capped CdSe QDs (from diameter of 2.5 to 5.2 nm). Although the values of CD anisotropy of cysteine-CdSe varied with their size (Table 1), changes of  $g_{\text{CD}}$  were small. No obvious correlation between diameter of CdSe and their  $g$  values was observed. The largest CD anisotropy was observed for L-Cys-CdSe nanoparticles with diameter of  $D = 4.4$  nm ( $-2.1 \times 10^{-4}$  at 580 nm). Due to differences in capping ligands, CD profiles and QD diameters made it unfeasible to directly compare our data with previously reported

**TABLE 1. CIRCULAR DICHROISM ANISOTROPY FACTORS OF L-CYS-CdSe QDs**

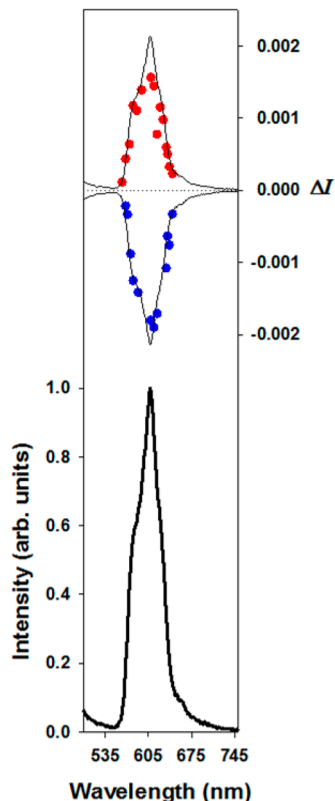
$D^a$	$\lambda_{\max}^b$	$g_{\text{CD}}^c / \lambda_{\text{CD}}^d$	$\lambda_{\text{CD}}^e / g_{\text{CD}}^c$
2.5	514.8	$0.6 \times 10^{-4} / 484.6$	$-0.4 \times 10^{-4} / 446.0$
2.9	543.0	$0.7 \times 10^{-4} / 548.8$	$-0.8 \times 10^{-4} / 532.2$
3.2	559.4	$1.2 \times 10^{-4} / 530.4$	$-1.2 \times 10^{-4} / 549.0$
3.6	574.2	$0.6 \times 10^{-4} / 474.6$	$-0.5 \times 10^{-4} / 446.0$
4.1	588.8	$1.7 \times 10^{-4} / 560.8$	$-1.9 \times 10^{-4} / 580.0$
4.4	596.2	$1.9 \times 10^{-4} / 569.0$	$-2.1 \times 10^{-4} / 587.8$
4.8	604.4	$1.3 \times 10^{-4} / 578.0$	$-1.1 \times 10^{-4} / 596.4$
5.2	613.4	$1.2 \times 10^{-4} / 592.6$	$-2.2 \times 10^{-4} / 575.0$

<sup>a</sup> Diameter determined by Peng's equation from the absorption spectrum (nm).<sup>b</sup> Band gap absorption (nm). <sup>c</sup> CD anisotropy *g*-factors. <sup>d,e</sup> Wavelengths of the most intense positive and negative CD bands (nm).**Figure 4.** Molar CD spectra of L-Cys-CdSe QDs of  $\varnothing = 2.5$  nm (red and magenta curves) and  $\varnothing = 5.2$  nm (blue curve). Both spectra were measured at  $A(\lambda_{\text{exc}}) = 0.85$ .

CD dissymmetry values of CdSe prepared by aqueous synthesis in the presence of chiral capping ligands.<sup>27</sup>

**Molar CD.** To compare the CD signal of Cys-CdSe with different diameters, the CD ellipticities (millidegree) have been converted into molar CD (delta epsilon) according to Beer–Lambert Law taking into account their concentration and cuvette path length. The intensity of the molar CD spectra of L-Cys-CdSe QDs increased dramatically with increasing diameter (Figure S10). As illustrated in Figure 4, the Cys-CdSe of  $\varnothing = 2.5$  nm exhibited the strongest Cotton effect of  $+4.07 \text{ M}^{-1} \text{ cm}^{-1}$  (385.8 nm), whereas  $-73.9 \text{ M}^{-1} \text{ cm}^{-1}$  (500.8 nm) was detected for  $\varnothing = 5.2$  nm. Doubling the size of Cys-CdSe thus increased the intensity of the most intense CD band  $\approx 18$ -fold, while the surface area of the CdSe nanoparticle increased only 4.3-fold. These results suggest that a type of cooperativity between cysteine ligands or orientation pattern also contributed to the intensity of the CD signal.

**Circularly Polarized Luminescence (CPL).** We have utilized CPL, the emission analog of CD, to further investigate the influence of the helicity in the compounds of interest on the chiroptical properties. Previously reported chiral QDs prepared in the presence of chiral thiol ligands did not show a CPL signal.<sup>22</sup> CPL was only observed for CdS prepared from scratch in a nanocage of an apoferritin.<sup>25</sup> CPL induced by chiral capping ligand has not been observed previously. The circularly polarized luminescence ( $\Delta I$ ) and total luminescence ( $I$ ) spectra measured for L-cysteine- and D-cysteine capped CdSe QDs in aqueous solutions at 295 K are shown in Figure 5.

**Figure 5.** CPL (upper curves) and total luminescence (lower curve) spectra of aqueous solution L-Cys-CdSe (red dots,  $\varnothing = 2.9$  nm) and D-Cys-CdSe (blue dots,  $\varnothing = 2.9$  nm) QDs ( $[\text{CdSe}] = 1 \text{ mM}$ , 295 K), upon excitation at 451 nm, respectively.

The degree of circularly polarized luminescence is given by the luminescence dissymmetry ratio,  $g_{\text{lum}}(\lambda) = 2\Delta I/I = 2(I_L - I_R)/(I_L + I_R)$ , where  $I_L$  and  $I_R$  refer, respectively, to the intensity of left and right circularly polarized emissions (refs 29–31 and references therein). The solid lines in the CPL plot are presented to show the luminescence spectral line shape. As usual for most chiral organic chromophores and transition metal complexes,  $|g_{\text{lum}}|$  that were obtained are small:  $+0.003$  and  $-0.004$  for L-cysteine- and D-cysteine capped CdSe QDs, as determined at the maximum emission wavelength, respectively. Although the  $g_{\text{lum}}$  values are very small (a value equal to  $\sim 0.003$  corresponding to light that is only 0.3% circularly polarized), opposite CPL signals were measured for the two QDs having opposite configuration at the chiral center of the capping cysteine ligand. This result confirms that the L-cysteine- and D-cysteine capped CdSe QDs solutions in water exhibit an active CPL signal and also that L- and D-cysteine induced modular chiroptical properties in achiral CdSe QDs (*i.e.*, the emitted light is polarized in opposite directions for the two enantiomeric forms of the QDs). This is the first example of chiral ligand induced CPL in semiconductor QD nanocrystals.

**Magic Angle Spinning Solid State NMR (MAS ssNMR).** To explore the interactions between cysteine capping

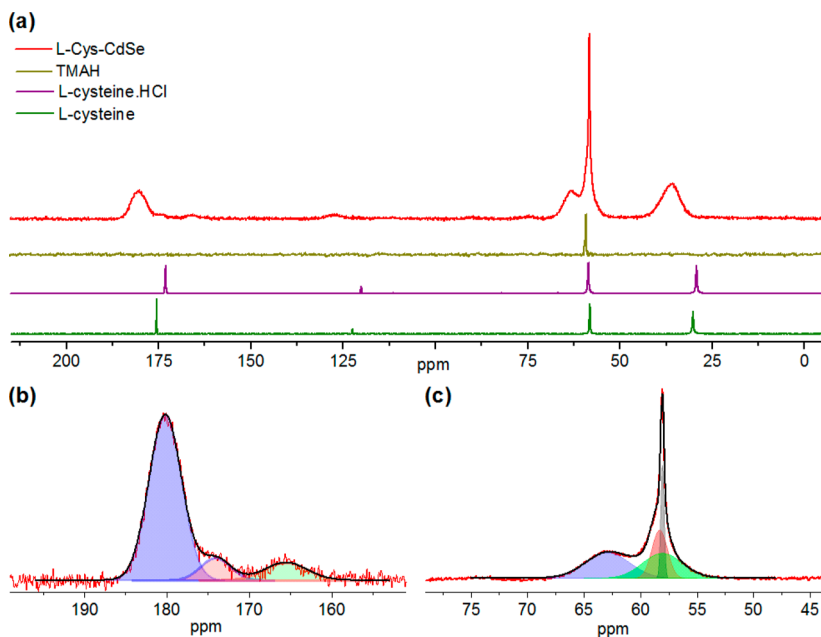


**Figure 6.** (a) 1D <sup>13</sup>C MAS ssNMR spectra of L-cysteine-CdSe QDs ( $\phi = 2.9$  nm), TMAH, L-cysteine.HCl, and L-cysteine. (b) Carbonyl region, and (c) C $\alpha$  region of <sup>13</sup>C MAS ssNMR spectrum of L-Cys-CdSe QDs (solid red line) and their fits. MAS ssNMR spectra were acquired on a 600 MHz Avance III Bruker NMR spectrometer at 299 K and 8.0 kHz MAS frequency.

ligands and the surface of CdSe QDs, we performed <sup>13</sup>C magic angle spinning solid state NMR experiments on L-cysteine capped CdSe QDs ( $\phi = 2.9$  nm) and compared them with <sup>13</sup>C MAS ssNMR spectra of L-cysteine hydrochloride and L-cysteine zwitterion (Figure 6). MAS ssNMR can distinguish between different conformations and binding modes of cysteine on the CdSe surface.<sup>15,32</sup> Optical activity induced in QDs by multipoint anchoring of chiral organic ligands has been postulated and supported by theoretical calculations previously.<sup>16</sup>

The spectra of cysteine and cysteine hydrochloride displayed three narrow peaks corresponding to C $\beta$ , C $\alpha$ , and C=O carbons. On the other hand, the <sup>13</sup>C ssNMR spectrum of cysteine-capped CdSe QDs exhibited a complicated profile with several broad peaks. Heterogeneous peak broadening originated from the size and shape heterogeneity of CdSe QDs and conformational heterogeneity of cysteine ligands attached to CdSe surface. Using a multiple peak fitting function in the OriginPro software, we have identified one peak in C $\beta$  carbon region, four peaks in C $\alpha$  carbon region, and three peaks in the carbonyl carbon region. The <sup>13</sup>C chemical shifts are summarized in Table 2.

The observed downfield shift of the C $\beta$  carbon ( $>5$  ppm in comparison to free cysteines) confirmed the attachment of cysteine to CdSe surface and absence of free cysteines. Three peaks observed in the carbonyl region have been potentially assigned as carboxylate (COO<sup>-</sup> at 180.2 ppm), carboxylic acid (COOH at 174.1 ppm) and carboxylate-CdSe complex (COO-CdSe at 165.6 ppm). Although four peaks have been identified in the C $\alpha$  region, the sharp peak at

**TABLE 2.** <sup>13</sup>C MAS ssNMR Shifts of L-Cysteine·HCl, L-Cysteine, and L-Cys-CdSe<sup>a</sup>

	C=O	C $\alpha$	C $\beta$
L-cysteine	175.5	58.1	30.2
L-cysteine.HCl	172.8	58.3	29.1
L-Cys-CdSe	180.2, 174.1, 165.6	62.9, 58.0, 58.3	35.7

<sup>a</sup> <sup>13</sup>C chemical shifts are reported in ppm with adamantane as an external standard referenced to DSS. L-Cys-CdSe chemical shifts were determined by signal fitting.

58.1 ppm belongs to tetramethylammonium hydroxide (TMAH, Figure 6: dark yellow curve). TMAH has been used as a base in the synthesis of cysteine-CdSe from OA-CdSe. Since spectra were acquired utilizing cross-polarization from <sup>1</sup>H to <sup>13</sup>C, the areas under the signals are not precisely proportional to the number of carbon nuclei. Overall, the <sup>13</sup>C ssNMR data suggested the bidentate interaction between cysteine and the surface of CdSe QDs probably involving thiol and carboxylate functional groups.

**Theoretical Simulations of the CD Spectra of Cysteine-CdSe Nanoclusters.** Theoretical simulations of the CD spectra were carried out to independently verify the origin of the observed CD signals. 'Magic size' (CdSe)<sub>13</sub> nanoclusters<sup>33</sup> were used as models for the QDs. While much smaller than the QDs investigated experimentally, the small size is necessary to keep the computations tractable, in particular since a large number of excited states has to be computed for an adequate representation of the UV and CD spectra (see below). All computations were done with Gaussian 09.<sup>34</sup> Model (CdSe)<sub>13</sub> nanoclusters were constructed based on the lowest energy optimized structure reported by

Azpiroz *et al.*<sup>35</sup> The geometry was optimized at the DFT level using dispersion corrected PBE/PBE<sup>36</sup> density functional and sbkj-c-VDZ basis set/ECP<sup>37,38</sup> with two additional d functions on Se atoms ( $\xi = 0.475412, 0.207776$ ),<sup>39</sup> which we denote sbkj-c-DZP\*. Conductor-like polarized continuum model (CPCM) was used to simulate aqueous environment, with default Gaussian 09 parameters for water. The optimized geometries of  $(\text{CdSe})_{13}$  nanoclusters (given in Supporting Information, Table S4) are in very good agreement with the previous reports.<sup>35</sup> Since the minimum energy  $(\text{CdSe})_{13}$  nanocluster lacks mirror symmetry, the optimization yields one of the enantiomers with a nonzero CD signal. To eliminate this intrinsic CD, which is not experimentally observed, racemic mixture was simulated by creating the opposite enantiomer as a mirror image of the optimized structure. Alternatively, an achiral, local minimum structure of  $(\text{CdSe})_{13}$  cluster<sup>35</sup> with the  $C_{3v}$  symmetry was also considered (see Supporting Information). With the implicit solvent model for water, the optimization could not maintain the  $C_{3v}$  symmetry, but converged to a  $C_s$  structure, which is nevertheless still achiral. The excited states of the  $(\text{CdSe})_{13}$  nanoclusters were calculated at TDDFT B3LYP/sbjk-c-VDZ\*/CPCM level.

L-Cys- and D-Cys- $(\text{CdSe})_{13}$  complexes were constructed using the  $(\text{CdSe})_{13}$  nanoclusters optimized as described above. With Cd and Se atoms held fixed, the L- and D-Cys geometries were further optimized using B3LYP hybrid density functional with 6-31+G(d) basis set for all Cys atoms (C, O, N, H, S) and sbkj-c-VDZ\* for Cd and Se. Note that freezing the CdSe cluster structure excluded any geometry distortions due to the ligand as possible cause of the induced chirality. Zwitterionic forms of L- and D-Cys were considered to mimic experimental conditions, and CPCM model was again used to simulate the aqueous environment. The optimized Cys- $(\text{CdSe})_{13}$  complexes are shown in Figure 7. See Supporting Information Figure S15 for the alternative ( $C_s$ ) cluster structure.

The excited states of the complexes were calculated at the same level of theory (B3LYP/6-31+G(d)/sbkj-c-VDZ\*/CPCM). The UV-vis absorption intensities were calculated using dipole length formalism, while for CD rotational strength the dipole velocity gauge was used. In both cases, the spectral contours were simulated by assigning Gaussian bandshapes with 25 nm width to all transitions.

Figure 8 shows the simulated UV-vis and CD spectra of L-Cys- and D-Cys- $(\text{CdSe})_{13}$  nanoclusters. The shape of the UV-vis absorption spectrum is in a very good correspondence with experimental data (Figures 2 and 3), though shifted to shorter wavelengths as expected for a smaller particle (the average diameter of the  $(\text{CdSe})_{13}$  is about 0.9 nm). As anticipated, the  $(\text{CdSe})_{13}$  exhibits a substantial CD signal (Figure S12). For this reason, as detailed above, a racemic mixture of

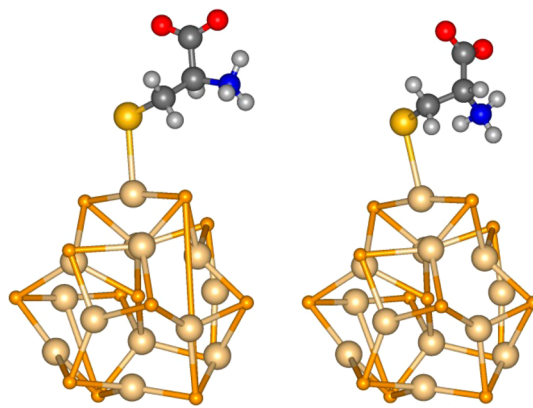


Figure 7. Optimized geometries of (left) L-Cys- $(\text{CdSe})_{13}$  and (right) D-Cys- $(\text{CdSe})_{13}$  nanoclusters.

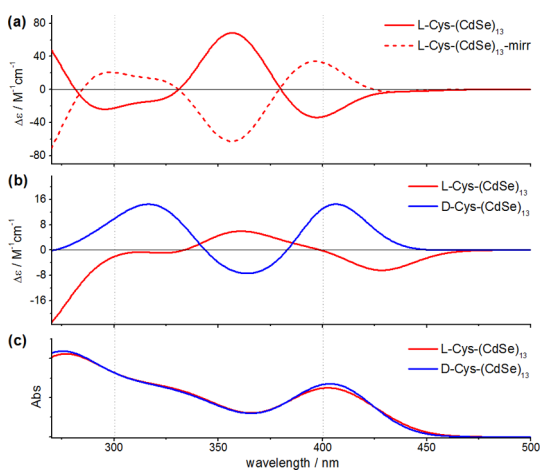


Figure 8. Theoretical simulations of CD and UV-vis spectra for model Cys-CdSe QDs: (a) calculated CD spectra of the L-Cys complex with the optimized  $(\text{CdSe})_{13}$  cluster (solid red curve) and with the opposite enantiomer of  $(\text{CdSe})_{13}$  (dashed red curve); (b) calculated CD spectra of L-Cys- $(\text{CdSe})_{13}$  (red curve) and D-Cys- $(\text{CdSe})_{13}$  (blue curve) corrected for the chirality of model  $(\text{CdSe})_{13}$  structures by adding the spectra of two  $(\text{CdSe})_{13}$  enantiomers (curves in (a) for L-Cys- $(\text{CdSe})_{13}$ ); (c) calculated UV-vis absorption spectra of L-Cys- $(\text{CdSe})_{13}$  (red curve) and D-Cys- $(\text{CdSe})_{13}$  (blue curve) of the same enantiomer of  $(\text{CdSe})_{13}$  nanocluster.

the nanoclusters was simulated by constructing a mirror image of the optimized geometry. The true CD signal due to the attachment of the cysteine molecule was then isolated by adding the spectra computed for the cysteine complexes with both enantiomers of the nanocluster. As shown in Figure 8b, the CD spectra calculated in this way qualitatively reproduce the general features measured experimentally for the capped CdSe QDs. A negative couplet CD corresponding to the excitonic absorption band ( $\sim 400$  nm) is calculated for LCys- $(\text{CdSe})_{13}$  as seen experimentally for the quantum dots prepared from TOPO/OA-CdSe (Figure 2b) as well as the smallest one investigated prepared from OA-CdSe. The opposite, positive couplet, is calculated for D-Cys- $(\text{CdSe})_{13}$  complex, as also observed experimentally (Figure 2b). Since cysteine itself does not have any UV transitions computed above  $\sim 230$  nm (Figure S13), the

predicted CD as shown in the 250–450 nm range is therefore entirely due to the CdSe nanoclusters, whose CD after correcting for the 'racemic' mixture, is induced by the interaction with the chiral cysteine.

The simulations also provided insights into the physical origin of the induced CD. From the molecular orbitals predominantly involved in the excitonic band transitions, the occupied ones, including HOMO, were generally delocalized over both the  $(\text{CdSe})_{13}$  cluster (Supporting Information, Figure S14) and the ligand. By contrast, the virtual orbitals (LUMO, LUMO+1, LUMO+2) stayed essentially localized on the former. The hybridization of the CdSe highest occupied orbitals with orbitals of the chiral ligand therefore appears to be the primary source of the induced chirality in  $(\text{CdSe})_{13}$  nanoclusters.<sup>40–43</sup> As the CdSe nanocluster geometries in the Cys- $(\text{CdSe})_{13}$  complex were fixed to the energy minimum of the bare nanocluster, the computed induced CD could not originate from the distortion of the  $(\text{CdSe})_{13}$  structure by the ligand. While in reality such structural distortion may contribute to the induced CD, for our small model clusters this effect would likely be severely overestimated as the relative degree of distortion is expected to be much less for larger QDs. Furthermore, since the model structures contained only a single cysteine per CdSe nanocluster, the simulations show that the general observed CD patterns were not due to any cooperative ligand effect. On the other hand, the interaction between Cys ligands could be responsible for the magnitude of the signal (see above), as well as, in combination with potentially different structural arrangements, for the qualitatively distinct CD bandshapes depending on the synthetic method (Figure 3).

Finally, to directly test the effect on the inherent chirality of the model CdSe clusters and its correction by a racemic mixture, we have also simulated the CD spectra for Cys complexes with achiral  $(\text{CdSe})_{13}$  clusters (Figure S15). The induced CD of similar magnitude and sign pattern corresponding to the excitonic band was

again observed. However, the simulations with the achiral  $(\text{CdSe})_{13}$  clusters also showed some important differences (Figure S15) implying that they are not as good models for the experimental QDs as the minimum energy ones (Figure 7). This can be expected, since the QDs are likely to be approximately spherical, while the  $C_s$  cluster structure is more of a planar slab (Figure S15). The differences indicated that the CD as well as UV spectra, despite their inherently low resolution, are sensitive to the details of the QD structure and its interactions with the ligand.

## CONCLUSIONS

The L- and D-enantiomers of amino acid cysteine induced opposite CD and CPL signals in CdSe QDs. This is the first example of ligand induced CPL in QDs. The CD spectroscopic properties and CD anisotropy varied with the size of CdSe nanocrystals. The largest CD anisotropy was detected for  $\varnothing = 4.4$  nm CdSe nanoparticles. Solid state NMR experiments suggested bidentate interaction between cysteine and the surface of CdSe. Theoretical simulations of the CD spectra for model Cys- $(\text{CdSe})_{13}$  nanoclusters qualitatively reproduced the experimental data, thus providing an independent verification of the ligand induced chirality in CdSe nanoparticles. The calculations further indicated that the induced CD is predominantly due to hybridization of the ligand HOMO with the QD valence band states and that the CD, along with the UV spectra, are quite sensitive to the details of structure and ligand-QD interactions. This implies that CD spectroscopic studies combined with theoretical simulations may lead to better fundamental understanding of the ligand induced chirality as well as structural and energetic aspects of the QD-ligand interaction, allowing for systematic and rational improvements in design and functionality. Such optimized design and modulation of chiroptical properties will likely lead to novel applications in chiroptical memory, chiral biosensing and chiroptical nanomaterials.

## METHODS

All reagents were purchased from Sigma-Aldrich and were used without any further purification. Water was obtained from Milli-Q system with a resistivity of 18.2  $\text{M}\Omega\cdot\text{cm}$ . OA-CdSe and TOPO/OA-CdSe QDs were synthesized using a modified literature procedure by Zou *et al.* (see Supporting Information).<sup>44</sup>

**Synthesis of Cys-CdSe.** Cysteine hydrochloride monohydrate (0.2 g) was dissolved in DI water (20 mL,  $[\text{Cys}] = 0.056$  M). The pH of the resulting solution was adjusted to 12.0 with tetramethylammonium hydroxide (TMAH). A solution of OA-CdSe QDs in toluene (12 mL, 0.03 mM,  $A_{(515\text{ nm})} = 2.0$ ;  $\varnothing = 2.5$  nm) was added to the cysteine solution, and the reaction mixture was deoxygenated and stirred at 20 °C under nitrogen in the absence of light for 24 h. The Cys-CdSe transferred to the bottom aqueous phase. The reaction mixture was left to stand for 1 h to allow the phases to separate. The bottom aqueous layer was taken out with a syringe, and Cys-CdSe QDs were purified by precipitation with

acetone/DI water (8:1, 2×). The purified Cys-CdSe QDs were dissolved in DI H<sub>2</sub>O and stored at 20 °C in the dark.

**UV–Vis Absorption Measurements.** UV–vis absorption spectra were collected at 20 °C using a Jasco V-600 UV–vis double beam spectrophotometer equipped with a single position Peltier temperature control system. A quartz cuvette with a 1 cm path length was used for all UV–vis experiments.

**Circular Dichroism (CD) and Fluorescence Detected Circular Dichroism (FDCD).** CD spectra were recorded at 20 °C using a Jasco J-815 spectropolarimeter equipped with a single position Peltier temperature control system. Conditions were as follows: scanning speed 100 nm/min, data pitch 0.5 nm, DIT 1 s, and bandwidth 4 nm. A quartz cuvette with a 1 cm path length was used for all CD experiments. Each CD spectrum was an average of at least 15 scans. FDCD spectra were recorded at 20 °C using a Jasco J-815 spectropolarimeter equipped with a single position FDCD Peltier temperature control system and a FDCD-465 attachment combining both a cylindrical cell and an

elliptical cylinder mirror. Conditions were as follows: scanning speed 100 nm/min, data pitch 0.5 nm, DIT 1 s, bandwidth 6 nm, 580 nm filter, and masks No7. Each FDCD spectrum was an average of at six scans.

**Fluorescence Measurements.** Emission spectra were recorded at 20 °C using a Varian fluorescence spectrophotometer equipped with a four position Peltier temperature control system using a scan rate of 600 nm/min, excitation wavelength 450 nm, with 5.0 nm excitation slit, and 5.0 nm emission slit. A quartz cuvette with a 1 cm path length was used.

**Circularly Polarized Luminescence (CPL).** CPL and total luminescence spectra were recorded on an instrument described previously,<sup>45</sup> operating in a differential photon-counting mode. The light source for excitation was a continuous wave 1000 W xenon arc lamp from a Spex Fluorolog-2 spectrophotometer, equipped with excitation and emission monochromators with dispersion of 4 nm/mm (SPEX, 1681B). To prevent artifacts associated with the presence of linear polarization in the emission,<sup>46</sup> a high quality linear polarizer was placed in the sample compartment, and aligned so that the excitation beam was linearly polarized in the direction of emission detection (z-axis). The key feature of this geometry is that it ensures that the molecules that have been excited and that are subsequently emitting are isotropically distributed in the plane (x,y) perpendicular to the direction of emission detection. The optical system detection consisted of a focusing lens, long pass filter, and 0.22 m monochromator. The emitted light was detected by a cooled EMI-9558B photomultiplier tube operating in photon-counting mode. All measurements were performed with quartz cuvettes with a path length of 1.0 cm.

**Transmission Electron Microscopy (TEM).** Samples for TEM were prepared by ultrasonic dispersion of the CdSe nanoparticles in toluene and water for the oleic acid and cysteine capped particles, respectively. The suspension was then drop-cast onto carbon-coated copper grids and dried in air. Imaging was performed on an FEI Tecnai G2 F20 scanning transmission electron microscope (STEM) operating at 200 kV.

**Magic Angle Spinning Solid State NMR (MAS ssNMR).** MAS ssNMR experiments were carried out on a 600 MHz Avance III Bruker NMR spectrometer equipped with a 3.2 mm  $E^{\text{free}}$  triple resonance HCN probe. Three standards (L-cysteine, L-cysteine hydrochloride, tetramethylammonium hydroxide) and L-cysteine capped CdSe QDs were packed into 4 mm Bruker rotors. To prepare the ssNMR sample, L-cysteine capped CdSe QDs were lyophilized overnight from water. One dimensional (1D)  $^{13}\text{C}$  ssNMR spectra were acquired using  $^1\text{H}$ – $^{13}\text{C}$  cross-polarization (CP) and  $^1\text{H}$  decoupling during acquisition. For the CdSe QDs,  $^1\text{H}$ – $^{13}\text{C}$  CP was achieved with a 70–100% ramped 63 kHz  $^1\text{H}$  and 50 kHz  $^{13}\text{C}$  pulses for 2.0 ms. Spectra was acquired for 20–40 ms with 78 kHz of two-pulse phase modulated (TPPM)  $^1\text{H}$  decoupling. For the standards, 16–128 transients were signal averaged. L-Cysteine capped CdSe QDs  $^{13}\text{C}$  spectrum took ~19 h to acquire (24 000 transients with 2.7 s recycle delay). Experiments were performed at 26 °C (variable temperature set point) and 8.0 kHz MAS frequency. All spectra were externally referenced to DSS using the adamantane downfield  $^{13}\text{C}$  peak at 40.48 ppm.<sup>47</sup> Data were processed with TopSpin.

**Conflict of Interest:** The authors declare no competing financial interest.

**Supporting Information Available:** Synthetic procedures; experimental CD, FDCD, UV–vis absorption and emission spectra of Cys-CdSe; calculated CD spectra of (CdSe)<sub>13</sub> and D- and L-cysteines. This material is available free of charge via the Internet at <http://pubs.acs.org>.

**Acknowledgment.** This work was supported by U.S. Department of Energy, Office of Basic Energy Sciences, Division of Materials Sciences and Engineering under Award DE-FG02-10ER46728 and by University of Wyoming Start-up Funds (M.B.). M.B. and U.T. thank the NSF Graduate STEM Fellows in K-12 Education (GK-12) Program (DGE-0948027). G.M. thanks the National Institute of Health, Minority Biomedical Research Support (1 SC3 GM089589-03 and 3 S06 GM008192-27S1) and the Henry Dreyfus Teacher-Scholar Award for financial support,

whereas K.K.D. thanks the NIH (MARC Grant 2T34GM008253-26) for a research fellowship. J.K. acknowledges the support of the National Science Foundation CAREER 0846140 grant.

## REFERENCES AND NOTES

- Gautier, C.; Bürgi, T. Chiral Nanoparticles. In *Chirality at the Nanoscale*; Wiley-VCH Verlag GmbH & Co. KGaA: Weinheim, 2009; pp 67–91.
- Ben-Moshe, A.; Maoz, B. M.; Govorov, A. O.; Markovich, G. Chirality and Chiroptical Effects in Inorganic Nanocrystal Systems with Plasmon and Exciton Resonances. *Chem. Soc. Rev.* **2013**, *42*, 7028–7041.
- Govorov, A. O.; Fan, Z. Y.; Hernandez, P.; Slocik, J. M.; Naik, R. R. Theory of Circular Dichroism of Nanomaterials Comprising Chiral Molecules and Nanocrystals: Plasmon Enhancement, Dipole Interactions, and Dielectric Effects. *Nano Lett.* **2010**, *10*, 1374–1382.
- Hidalgo, F.; Noguez, C. Optically Active Nanoparticles: Fullerenes, Carbon Nanotubes, and Metal Nanoparticles. *Phys. Status Solidi B* **2010**, *247*, 1889–1897.
- Govan, J. E.; Jan, E.; Querejeta, A.; Kotov, N. A.; Gun'ko, Y. K. Chiral Luminescent CdS Nano-Tetrapods. *Chem. Commun.* **2010**, *46*, 6072–6074.
- Xia, Y.; Zhou, Y.; Tang, Z. Chiral Inorganic Nanoparticles: Origin, Optical Properties and Bioapplications. *Nanoscale* **2011**, *3*, 1374–1382.
- Fan, Z.; Govorov, A. O. Helical Metal Nanoparticle Assemblies with Defects: Plasmonic Chirality and Circular Dichroism. *J. Phys. Chem. C* **2011**, *115*, 13254–13261.
- Nakashima, T.; Kobayashi, Y.; Kawai, T. Optical Activity and Chiral Memory of Thiol-Capped CdTe Nanocrystals. *J. Am. Chem. Soc.* **2009**, *131*, 10342–10343.
- Layani, M. E.; Ben Moshe, A.; Varenik, M.; Regev, O.; Zhang, H.; Govorov, A. O.; Markovich, G. Chiroptical Activity in Silver Cholate Nanostructures Induced by the Formation of Nanoparticle Assemblies. *J. Phys. Chem. C* **2013**, *22240*–22244.
- Gautier, C.; Bürgi, T. Chiral Gold Nanoparticles. *ChemPhysChem* **2009**, *10*, 483–492.
- Dolamic, I.; Knoppe, S.; Dass, A.; Bürgi, T. First Enantioseparation and Circular Dichroism Spectra of Au-38 Clusters Protected by Achiral Ligands. *Nat. Commun.* **2012**, *3*, 798.
- Shukla, N.; Bartel, M. A.; Gellman, A. J. Enantioselective Separation on Chiral Au Nanoparticles. *J. Am. Chem. Soc.* **2010**, *132*, 8575–8580.
- Maoz, B. M.; van der Weegen, R.; Fan, Z.; Govorov, A. O.; Ellestad, G.; Berova, N.; Meijer, E. W.; Markovich, G. Plasmonic Chiroptical Response of Silver Nanoparticles Interacting with Chiral Supramolecular Assemblies. *J. Am. Chem. Soc.* **2012**, *134*, 17807–17813.
- Hidalgo, F.; Noguez, C. Optical Activity of Achiral Ligand SCH3 Adsorbed on Achiral Ag55 Clusters: Relationship between Adsorption Site and Circular Dichroism. *ACS Nano* **2012**, *7*, 513–521.
- Zhou, Y.; Yang, M.; Sun, K.; Tang, Z.; Kotov, N. A. Similar Topological Origin of Chiral Centers in Organic and Nanoscale Inorganic Structures: Effect of Stabilizer Chirality on Optical Isomerism and Growth of CdTe Nanocrystals. *J. Am. Chem. Soc.* **2010**, *132*, 6006–6013.
- Elliott, S. D.; Moloney, M. P.; Gun'ko, Y. K. Chiral Shells and Achiral Cores in CdS Quantum Dots. *Nano Lett.* **2008**, *8*, 2452–2457.
- Tohgha, U.; Varga, K.; Balaz, M. Achiral CdSe Quantum Dots Exhibit Optical Activity in the Visible Region upon Post-Synthetic Ligand Exchange with D- or L-Cysteine. *Chem. Commun.* **2013**, *49*, 1844–1846.
- Noguez, C.; Sánchez-Castillo, A.; Hidalgo, F. Role of Morphology in the Enhanced Optical Activity of Ligand-Protected Metal Nanoparticles. *J. Phys. Chem. Lett.* **2011**, *2*, 1038–1044.
- Sánchez-Castillo, A.; Noguez, C.; Garzón, I. L. On the Origin of the Optical Activity Displayed by Chiral-Ligand-Protected Metallic Nanoclusters. *J. Am. Chem. Soc.* **2010**, *132*, 1504–1505.

20. Govorov, A. O. Plasmon-Induced Circular Dichroism of a Chiral Molecule in the Vicinity of Metal Nanocrystals. Application to Various Geometries. *J. Phys. Chem. C* **2011**, *115*, 7914–7923.

21. Maoz, B. M.; Chaikin, Y.; Tesler, A. B.; Bar Elli, O.; Fan, Z.; Govorov, A. O.; Markovich, G. Amplification of Chiroptical Activity of Chiral Biomolecules by Surface Plasmons. *Nano Lett.* **2013**, *13*, 1203–1209.

22. Moloney, M. P.; Gun'ko, Y. K.; Kelly, J. M. Chiral Highly Luminescent CdS Quantum Dots. *Chem. Commun.* **2007**, 3900–3902.

23. Gallagher, S. A.; Moloney, M. P.; Wojdyla, M.; Quinn, S. J.; Kelly, J. M.; Gun'ko, Y. K. Synthesis and Spectroscopic Studies of Chiral CdSe Quantum Dots. *J. Mater. Chem.* **2010**, *20*, 8350–8355.

24. Zhou, R.; Wei, K.-Y.; Zhao, J.-S.; Jiang, Y.-B. Alternative Chiral Thiols for Preparation of Chiral CdS Quantum Dots Covered Immediately by Achiral Thiols. *Chem. Commun.* **2011**, *47*, 6362–6364.

25. Naito, M.; Iwahori, K.; Miura, A.; Yamane, M.; Yamashita, I. Circularly Polarized Luminescent CdS Quantum Dots Prepared in a Protein Nanocage. *Angew. Chem., Int. Ed.* **2010**, *49*, 7006–7009.

26. Yu, W. W.; Qu, L.; Guo, W.; Peng, X. Experimental Determination of the Extinction Coefficient of CdTe, CdSe, and CdS Nanocrystals. *Chem. Mater.* **2003**, *15*, 2854–2860.

27. Ben Moshe, A.; Szwarcman, D.; Markovich, G. Size Dependence of Chiroptical Activity in Colloidal Quantum Dots. *ACS Nano* **2011**, *5*, 9034–9043.

28. Nehira, T.; Tanaka, K.; Takakuwa, T.; Ohshima, C.; Masago, H.; Pescitelli, G.; Wada, A.; Berova, N. Development of a Universal Ellipsoidal Mirror Device for Fluorescence Detected Circular Dichroism: Elimination of Polarization Artifacts. *Appl. Spectrosc.* **2005**, *59*, 121–125.

29. Riehl, J. P.; Muller, G. Circularly Polarized Luminescence Spectroscopy and Emission-Detected Circular Dichroism. In *Comprehensive Chiroptical Spectroscopy*; John Wiley & Sons, Inc.: New York, 2012; pp 65–90.

30. Solntsev, K. M.; Bartolo, E.; Pan, G.; Muller, G.; Bommireddy, S.; Huppert, D.; Tolbert, L. M. Excited-State Proton Transfer in Chiral Environments: Photoracemization of BINOLs. *Isr. J. Chem.* **2009**, *49*, 227–233.

31. Riehl, J. P.; Muller, G. Circularly Polarized Luminescence Spectroscopy from Lanthanide Systems. In *Handbook on the Physics and Chemistry of Rare Earths*; Elsevier: Oxford, 2004; Vol. 34, pp 289–357.

32. Ratcliffe, C. I.; Yu, K.; Ripmeester, J. A.; Badruz Zaman, M.; Badarau, C.; Singh, S. Solid State NMR Studies of Photoluminescent Cadmium Chalcogenide Nanoparticles. *Phys. Chem. Chem. Phys.* **2006**, *8*, 3510–3519.

33. Wang, Y. Y.; Liu, Y. H.; Zhang, Y.; Wang, F. D.; Kowalski, P. J.; Rohrs, H. W.; Loomis, R. A.; Gross, M. L.; Buhro, W. E. Isolation of the Magic-Size CdSe Nanoclusters  $(\text{CdSe})_{13}(n\text{-Octylamine})_{13}$  and  $(\text{CdSe})_{13}(\text{Oleylamine})_{13}$ . *Angew. Chem., Int. Ed.* **2012**, *51*, 6154–6157.

34. Frisch, M. J.; Trucks, G. W.; Schlegel, H. B.; Scuseria, G. E.; Robb, M. A.; Cheeseman, J. R.; Scalmani, G.; Barone, V.; Mennucci, B.; Petersson, G. A., et al. *Gaussian 09*; Gaussian, Inc.: Wallingford, CT, 2009.

35. Azpiroz, J. M.; Matxain, J. M.; Infante, I.; Lopez, X.; Ugalde, J. M. A DFT/TDDFT Study on the Optoelectronic Properties of the Amine-Capped Magic  $(\text{CdSe})_{13}$  Nanocluster. *Phys. Chem. Chem. Phys.* **2013**, *15*, 10996–11005.

36. Perdew, J. P.; Burke, K.; Ernzerhof, M. Generalized Gradient Approximation Made Simple. *Phys. Rev. Lett.* **1996**, *77*, 3865–3868.

37. Stevens, W. J.; Krauss, M.; Basch, H.; Jasien, P. G. Relativistic Compact Effective Potentials and Efficient, Shared-Exponent Basis Sets for the Third-, Fourth-, and Fifth-Row Atoms. *Can. J. Chem.* **1992**, *70*, 612–630.

38. Schuchardt, K. L.; Didier, B. T.; Elsethagen, T.; Sun, L.; Gurumoorthi, V.; Chase, J.; Li, J.; Windus, T. L. Basis Set Exchange: A Community Database for Computational Sciences. *J. Chem. Inf. Model.* **2007**, *47*, 1045–1052.

39. Nguyen, K. A.; Pachter, R.; Day, P. N. Computational Prediction of Structures and Optical Excitations for Nanoscale Ultrasmall ZnS and CdSe Clusters. *J. Chem. Theory Comput.* **2013**, *9*, 3581–3596.

40. Moshe, A. B.; Markovich, G. Chiral Ligand-Induced Circular Dichroism in Excitonic Absorption of Colloidal Quantum Dots. *Isr. J. Chem.* **2012**, *52*, 1104–1110.

41. Govorov, A. O.; Gun'ko, Y. K.; Slocik, J. M.; Gerard, V. A.; Fan, Z.; Naik, R. R. Chiral Nanoparticle Assemblies: Circular Dichroism, Plasmonic Interactions, and Exciton Effects. *J. Mater. Chem.* **2011**, *21*, 16806–16818.

42. Chung, S.-Y.; Lee, S.; Liu, C.; Neuhauser, D. Structures and Electronic Spectra of CdSe-Cys Complexes: Density Functional Theory Study of a Simple Peptide-Coated Nanocluster. *J. Phys. Chem. B* **2008**, *113*, 292–301.

43. Lee, J. R. I.; Whitley, H. D.; Meulenber, R. W.; Wolcott, A.; Zhang, J. Z.; Prendergast, D.; Lovingood, D. D.; Strouse, G. F.; Ogitsu, T.; Schwegler, E., et al. Ligand-Mediated Modification of the Electronic Structure of CdSe Quantum Dots. *Nano Lett.* **2012**, *12*, 2763–2767.

44. Dai, Q.; Li, D.; Chen, H.; Kan, S.; Li, H.; Gao, S.; Hou, Y.; Liu, B.; Zou, G. Colloidal CdSe Nanocrystals Synthesized in Non-coordinating Solvents with the Addition of a Secondary Ligand: Exceptional Growth Kinetics. *J. Phys. Chem. B* **2006**, *110*, 16508–16513.

45. Brunet, E.; Jiménez, L.; de Victoria-Rodríguez, M.; Luu, V.; Muller, G.; Juanes, O.; Rodríguez-Ubis, J. C. The Use of Lanthanide Luminescence as a Reporter in the Solid State: Desymmetrization of the Prochiral Layers of  $\gamma$ -Zirconium Phosphate/Phosphonate and Circularly Polarized Luminescence. *Microporous Mesoporous Mater.* **2013**, *169*, 222–234.

46. Dekkers, H. P. J. M.; Moraal, P. F.; Timper, J. M.; Riehl, J. P. Optical Artifacts in Circularly Polarized Luminescence Spectroscopy. *Appl. Spectrosc.* **1985**, *39*, 818–821.

47. Morcombe, C. R.; Zilm, K. W. Chemical Shift Referencing in MAS Solid State NMR. *J. Magn. Reson.* **2003**, *162*, 479–486.